Experimental and Molecular Pathology 145 (2026) 105036

Contents lists available at ScienceDirect

Experimental and Molecular Pathology

journal homepage: www.elsevier.com/locate/yexmp

25-nitro-20-*epi*-vitamin D analogue with anti-proliferative and cytoprotective properties: Biological and pharmacological evaluation

Uxía Gómez-Bouzó [a,*], Carole Peluso-Iltis [b], Sandra Barreiro [c,d], Carlos Fernandes [e,f], Lieve Verlinden [g], Annemieke Verstuyf [g], Fernanda Borges [e,f,h], Natacha Rochel [b,*], Generosa Gómez [a], Yagamare Fall [a]

[a] Department of Organic Chemistry and Instituto de Investigación Sanitaria Galicia Sur (IISGS), Campus Lagoas-Marcosende, University of Vigo, 36310 Vigo, Spain
[b] Université de Strasbourg, CNRS, Inserm, IGBMC UMR 7104- UMR-S 1258, F-67400 Illkirch, France
[c] Associate Laboratory i4HB – Institute for Health and Bioeconomy, Faculty of Pharmacy, University of Porto, R. Jorge de Viterbo Ferreira 228, 4050-313 Porto, Portugal
[d] UCIBIO – Applied Molecular Biosciences Unit, REQUIMTE, Laboratory of Toxicology, Department of Biological Sciences, Faculty of Pharmacy, University of Porto, R. Jorge de Viterbo Ferreira 228, 4050-313 Porto, Portugal
[e] MedInUP-Rise-Health, University of Porto, 4200-319 Porto, Portugal
[f] Department of Biomedicine-Pharmacology and Therapeutics Unit, Faculty of Medicine, University of Porto, 4200-319 Porto, Portugal
[g] Clinical and Experimental Endocrinology, Department of Chronic Diseases and Metabolism, KU Leuven, Herestraat 49, 3000 Leuven, Belgium
[h] Department of Chemistry and Biochemistry, Faculty of Sciences, University of Porto, R. Campo Alegre s/n, 4169-007 Porto, Portugal

ARTICLE INFO

Keywords:
Calcitriol
Cytotoxicity
Oxidative stress
VDR binding
Anti-proliferative activity

ABSTRACT

We report the synthesis and pharmacological evaluation of **UG-635**, a novel 25-nitro vitamin D analogue bearing a 20-epimeric configuration. Cytotoxicity studies in SH-SY5Y neuroblastoma and HepG2 hepatocarcinoma cells showed that **UG-635** is well tolerated at low concentrations but reduces viability at higher doses. Importantly, **UG-635** demonstrated protective effects against oxidative stress in neuronal cells and exhibited anti-proliferative activity in breast cancer (MCF7) and osteoblast (MC3T3-E1) models, with efficacy comparable to calcitriol. Structural and crystallographic analyses revealed efficient binding to the vitamin D receptor (VDR), stabilizing its active conformation through favorable interactions with anchoring histidines. These findings highlight **UG-635** as a promising vitamin D analogue with potential pharmacological relevance in cancer and neurodegenerative disease contexts, combining anti-proliferative and cytoprotective properties.

1. Introduction

The active metabolite of vitamin D, 1α,25-dihydroxyvitamin D_3 (1α,25$(OH)_2D_3$, calcitriol, Fig. 1), is crucial for maintaining calcium balance in the body and exhibits both anti-proliferative and anti-inflammatory properties. It has been shown to reduce symptom severity in preclinical models of autoimmune diseases and various cancers. However, achieving these therapeutic benefits necessitates supra-physiological doses of calcitriol, which can lead to hypercalcemia and calcification in different tissues. (Eelen et al., 2006; Posner and Kahraman, 2003; Ferronato et al., 2019)

To overcome these limitations, numerous analogues of calcitriol have been developed aiming to dissociate the desired non-calcemic activities from calcium mobilization. (Patel et al., 2025) Among them, C20

Abbreviations: 1α,25$(OH)_2D_3$, 1α,25-dihydroxyvitamin D_3; ABTS, 2,2′-azino-bis(3-ethylbenzothiazoline-6-sulfonic acid); DBU, 1,8-diazabicyclo[5.4.0]undec-7-ene; DIBAL-H, diisobutylaluminium hydride; DMEM, Dulbecco's Modified Eagle Medium; EDTA, ethylenediaminetetraacetic acid; FeNTA, iron(III)-nitrilotriacetate complex; FBS, fetal bovine serum; HBSS, Hank's balanced salt solution; HepG2, human hepatocarcinoma cell line; LBD, ligand binding domain; MAPK, mitogen-activated protein kinase; MC3T3-E1, mouse pre-osteoblast cell line; MCF7, human breast adenocarcinoma cell line; MEFs, murine embryonic fibroblasts; NEAA, nonessential amino acids; NF-κB, nuclear factor kappa B; NR, neutral red assay; Nrf2, nuclear factor erythroid 2–related factor 2; PBS, phosphate-buffered saline; PDC, pyridinium dichromate; PKC, protein kinase C; PDIA3, protein disulfide isomerase family A member 3; RA, retinoic acid; ROS, reactive oxygen species; SH-SY5Y, human neuroblastoma cell line; SRB, sulforhodamine B assay; TBAF, tetrabutylammonium fluoride; TBS, *tert*-butyldimethylsilyl; TES, triethylsilyl; TPA, 12-O-tetradecanoylphorbol-13-acetate; *t*-BHP, tert-butyl hydroperoxide; VDR, vitamin D receptor; zVDR, zebrafish vitamin D receptor; αMEM, alpha minimum essential medium..

* Corresponding authors.
E-mail addresses: ugomez@uvigo.gal (U. Gómez-Bouzó), rochel@igbmc.fr (N. Rochel).

https://doi.org/10.1016/j.yexmp.2026.105036
Received 13 October 2025; Received in revised form 6 February 2026; Accepted 11 February 2026
Available online 23 February 2026

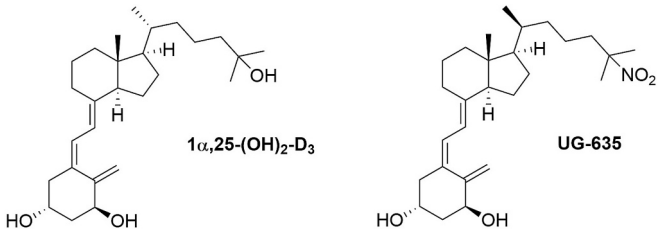

Fig. 1. Structures of **1α,25(OH)$_2$D$_3$** and 25-nitro-20-*epi* derivate (**UG-635**).

*epi*merization has emerged as a prominent structural modification. The 20-*epi* analogues display significantly enhanced anti-proliferative and immunomodulatory effects compared to calcitriol, while maintaining similar VDR affinity and reduced calcemic activity. This enhancement has been attributed to altered protein-ligand dynamics, including slower catabolism and improved stabilization of the VDR active conformation. (Binderup et al., 1991; Dilworth et al., 1994; Rochel et al., 2000; Rochel and Moras, 2011)

A second strategy involves the introduction of heteroatoms into the side chain of calcitriol to modulate physicochemical and metabolic properties. Notably, replacement of the C25 hydroxyl group—a key site for metabolic deactivation—has yielded analogues with altered binding and improved biological profiles (Ferronato et al., 2019; Rivadulla et al., 2013). In our previous work (Gómez-Bouzó et al., 2023), we reported that C25 nitro and amino derivatives of calcitriol retained potent anti-proliferative effects and VDR agonism, while showing altered hydrogen bonding and reduced interaction strength with anchoring residues.

In addition to these strategies, recent studies have revealed (Slominski et al., 2024a; Slominski et al., 2022; Slominski et al., 2024b; Slominski et al., 2020; Chaiprasongsuk et al., 2019) alternative vitamin D activation pathways involving CYP11A1, which generate biologically active hydroxyderivatives and lumisterol metabolites. These compounds act through the VDR as well as alternative nuclear receptors and have shown anticancer, antioxidant, and DNA-protective effects in skin and cancer models.

These findings, together with our previous results, support further exploration of nitro-substituted analogues as potential selective modulators of VDR activity.

Building on these insights, we now describe the synthesis, biological evaluation, and structural analysis of **UG-635** (Fig. 1), a novel C25 nitro vitamin D analogue bearing a 20-*epi* configuration.

2. Results and discussion

2.1. Design

We anticipated that the analogue **UG-635** could be synthesized from 20-*epi* alcohol **1**. The synthesis involves the construction of Grundmann's ketone **3**, followed by a Wittig−Horner coupling using phosphine oxide **4** to afford the target compound. The retrosynthetic analysis of **UG-635** is depicted in Scheme 1.

Alcohol **1**, featuring epimerization at C20, was synthesized from commercially available **Inhoffen-Lythgoe diol**. The 20-epimerization process involved the equilibrium of the corresponding aldehyde with DBU under reflux, followed by reduction with $NaBH_4$, as previously reported by Fujishima et al. (Fujishima et al., 1998)

Accordingly, allyl alcohol **2** was prepared as outlined in Scheme 2. 2,2,6,6-Tetramethyl-1-piperidinyloxy (TEMPO) oxidation of alcohol **1**, followed by Wittig reaction of the resulting aldehyde **5** afforded ester **6** in 69% overall yield over two steps. DIBAL-H reduction of ester **6** afforded allylic alcohol **2** in 99% yield.

The acetylation of allylic alcohol **2** afforded compound **7** in 97% yield. The Pd-allylic substitution of **7** to obtain the homoallylic nitro compound **8** was achieved in 60% yield by treating allylic acetate **7** with 2-nitropropane in the presence of $Pd(PPh_3)_4$ as the catalyst. Notably, the formation of two byproducts was observed, which will be detailed in the following section. Catalytic hydrogenation of **8** yielded the nitro derivative **9** in 80% yield. The desilylation of **9**, gave alcohol **10**, which by oxidation with PDC, afforded Grundmann's ketone **3** in 92% yield over two steps (Scheme 3).

The methodology for incorporating the nitro group at C25 was adapted from previous work in our research group (9), yielding the nitro derivative with a 90% yield. However, applying the same conditions to 20-*epi* allylic acetate **7** resulted in three different products (Scheme 4A). These findings indicate a *syn*-elimination pathway in the Pd-catalyzed elimination of allylic acetate **7**, proceeding *via* a *β*-elimination from the intermediate π-allylic Pd complex, forming the terminal conjugated diene system **11** (Scheme 4B). Additionally, the formation of a nitronic ester **13** and subsequent decomposition to carbonyl compound **12** was observed, suggesting *O*-alkylation occurred at the less substituted side of the π-allylpalladium intermediate (Scheme 4C). Notably, the stereochemistry of the nucleophilic allyl-Pd substitution reaction is influenced by the antiperiplanar placement of palladium, optimizing the transition state and minimizing steric interactions. These results suggest that anti-*β*-H-elimination does not occur in the naturally configure C20 allylic acetate.

With Grundmann's ketone **3** in hand, the stage was now set for the Wittig−Horner reaction with phosphine oxide **4** and the final desilylation to afford uneventfully 76% yield (2 steps) of the target compound

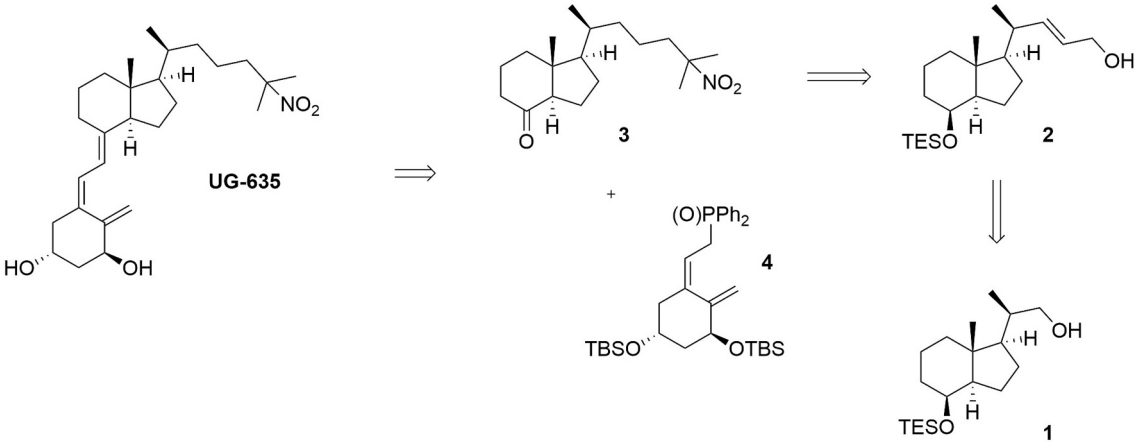

Scheme 1. Retrosynthetic analysis for **UG-635**.

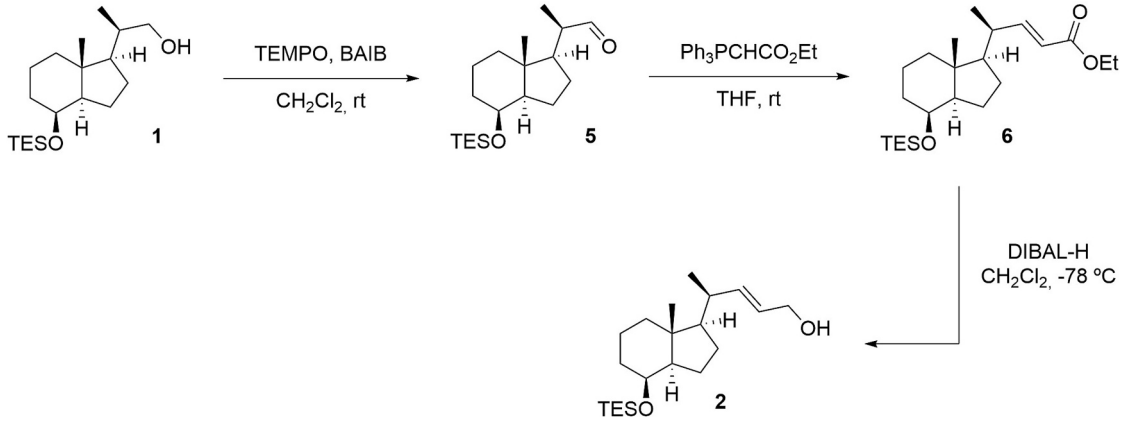

Scheme 2. Synthetic sequence to obtain allylic alcohol **2**.

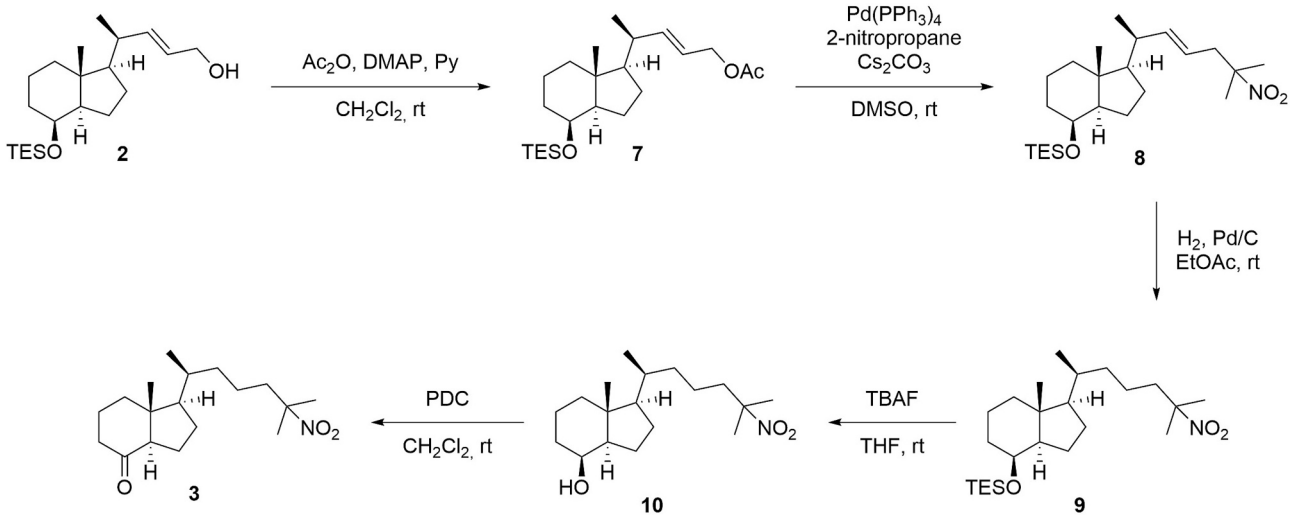

Scheme 3. Synthetic sequence to obtain Grundmann's ketone **3**.

UG-635 (Scheme 5).

2.2. Cellular studies

The cytotoxicity of **UG-635** and calcitriol was evaluated in both human neuroblastoma (SH-SY5Y) and hepatocarcinoma (HepG2) cell lines by assessing the metabolic activity, lysosomal activity, and cell mass, through the resazurin reduction, neutral red (NR) uptake, and sulforhodamine B (SRB) binding assays, respectively (Fig. 2). Both HepG2 and SH-SY5Y cell lines are frequently used in safety assessment of drugs. (Fernandes et al., 2018a)

In differentiated SH-SY5Y cells, a range of concentrations (0–50 μM) was tested in order to produce a more accurate dose-response curve, and to further select the concentrations to use in the followed protection studies. The data showed that **UG-635** did not affect cell viability for concentrations lower than 5 μM. More detailed, the treatment of SH-SY5Y cells with **UG-635** compound with concentrations equal to or higher than 6.25 μM caused a depletion of metabolic and lysosomal activities as well as cell mass (Fig. 2A-C). By comparing with **UG-635**, it is possible to observe that calcitriol exhibited lower cytotoxicity, since only caused depletion of viability for concentrations higher than 25 μM (Fig. 2A-C).

Regarding the cytotoxic profile of the compounds in HepG2 cells (Fig. 2D-F), only four concentrations (1, 10, 25, 50 μM) were tested to identify the potential hepatotoxic effect of these compounds. In all cases, the cytotoxicity of the tested compounds greatly increased for the higher concentrations tested, with the effects more noticeable for concentrations higher than 10 μM and particularly observed in the lysosomal activity and cell mass (Fig. 2E-F). Contrarily to what happened using neuroblastoma cells, it is also observed that, despite the increased cytotoxic effects, **UG-635** compound displayed a cytotoxic profile similar to that of calcitriol in HepG2 cells.

The screening of **UG-635** compound as well as calcitriol as protective agents against oxidative stress damage induced by different stressors was performed at 5 μM and measured using resazurin and SRB methods (Fig. 3). Different oxidative stress inducers were used, namely *tert*-butyl hydroperoxide (*t*-BHP) and iron (III) (FeNTA reagent). The *t*-BHP activates the opening of a nonspecific Ca^{2+} dependent pore in cell mitochondria as well as being a promotor of cell death, due to the activation of lipid peroxidation processes. Meanwhile, FeNTA reagent is a pro-oxidant involved in the generation of oxidative stress. Iron accumulation produces oxidative damage in neuroblastoma cells, namely due to its catalytic activity in Fenton reaction. (Fernandes et al., 2018b)

As shown in Fig. 3, cell treatment with the oxidative inducers caused a significant decrease in cell viability ($p < 0.0001$) when compared with non-treated cells at the end points of each experiment. The metabolic activity of SH-SY5Y cells was 64.5 ± 1.9% and 48.3 ± 13.9% after treatment with *t*-BHP (200 μM) and FeNTA (3 mM), respectively. Meanwhile, the cell mass was 64.1 ± 10.9% and 47.2 ± 6.1% for cells exposed to *t*-BHP (200 μM) and FeNTA (3 mM), respectively.

The pre-incubation of cells with both **UG-635** and calcitriol afforded protection against the effects of the stressors, with few exceptions where

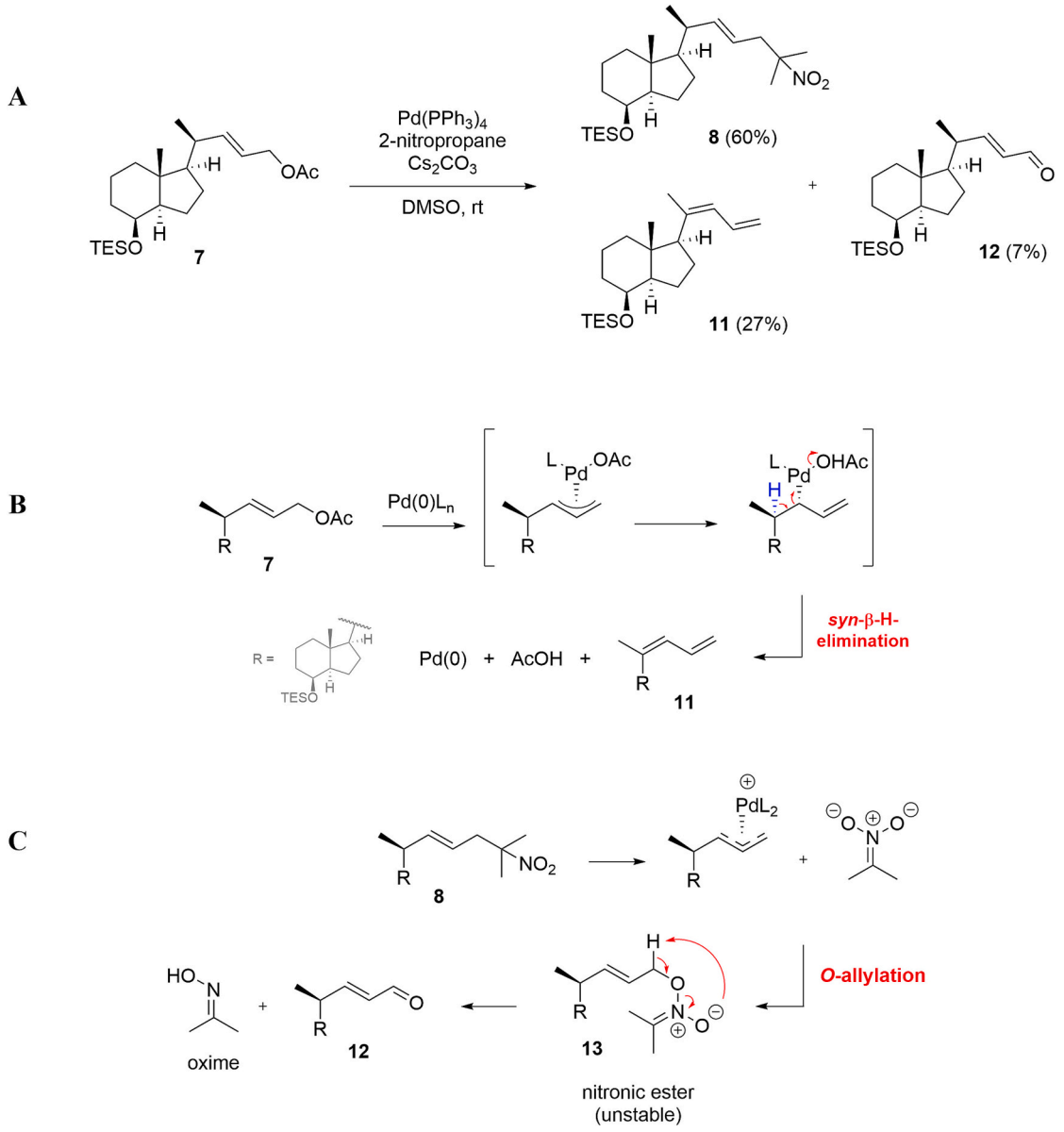

Scheme 4. (**A**) Tsuji-Trost reaction of allylic acetate **7**. (**B**) Formation of a terminal conjugated diene system **11** by the Pd-catalyzed elimination reaction of allylic acetate **7**. (**C**) Formation of a *α,β*-unsaturated aldehyde **12** by the Pd-catalyzed *O*-allylation reaction of nitro compound **8**.

non-significative effects in cell viability were observed. The use of **UG-635**-based compound caused an improvement of metabolic activity (73.4 ± 12.6%) against *t*-BHP aggression (64.1 ± 1.9%, Fig. 3A) as well as an increasing of cell mass (80.9 ± 7.9% and 54.0 ± 4.7%, Fig. 3B) when cells were treated with *t*-BHP (64.1 ± 10.8%, Fig. 3B) and iron(III) (47.2 ± 6.1%, Fig. 3D), respectively. Meanwhile, calcitriol (63.1 ± 6.6%) only led to an increase of cell mass against iron(III) aggression (Fig. 3D). To assess if the protective effect of **UG-635** and calcitriol is due to a direct interaction with stressors, or by chelating or antioxidant capacity, we performed a screening of their properties using cell-free ferrozine and ABTS radical scavenging methods, respectively. Both compounds did not show any antioxidant activity against ABTS radical (data not shown), while only **UG-635**-based compound showed a moderate capacity to chelate iron(II) (41.3 ± 8.9%). The data obtained in cell-free experiments could be due to the steric hindrance of bulky character of antioxidant and/or radical agent, which can avoid the neutralizing of the ABTS radical or probably the compounds protected the cells from damage caused by the stressors by indirect way, such as increasing the defenses of the cells or reducing the metabolization of the stressors.

It has been reported that 20-*epi* vitamin D exerts cytoprotective effects through a combination of rapid non-genomic and slower genomic mechanisms. (Voltan et al., 2023) The non-genomic actions are initiated at the plasma membrane *via* VDR and its associated protein PDIA3, leading to the activation of intracellular kinases such as mitogen-activated protein kinase (MAPK) and protein kinase C (PKC), as well as modulation of Ca^{2+} ion channels. (Nowak et al., 2023) These rapid signalling events contribute to early cellular adaptation to stress.

In parallel, 20-*epi* vitamin D regulates gene transcription through classical genomic pathways, influencing calcium homeostasis, redox balance, and cellular stress responses. (Nowak et al., 2023) For that, a key mechanism involves activation of the Nrf2 pathway, resulting in the upregulation of antioxidant and cytoprotective genes, including heme oxygenase-1 and glutathione S-transferases, thereby limiting ROS accumulation. Also, it can modulate inflammatory and stress-responsive pathways such as NF-κB and WNT signalling, further contributing to cellular homeostasis. Moreover, the Vitamin D–dependent cytoprotection has been linked to interactions between VDR and Klotho, which

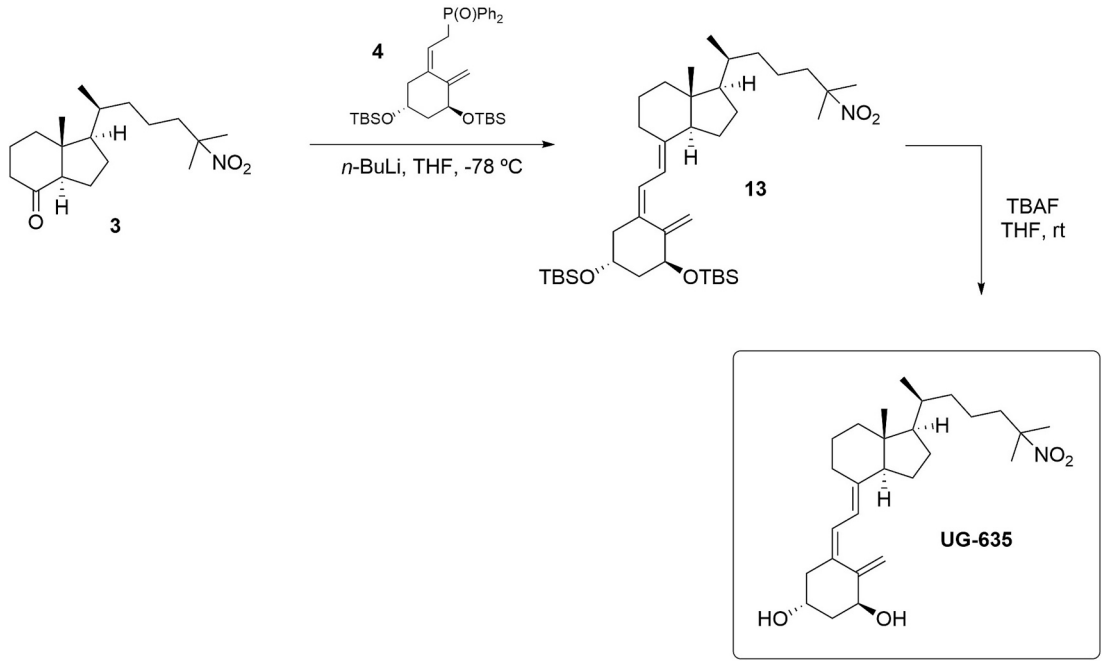

Scheme 5. Synthetic sequence to obtain the analogue **UG-635.**

collectively regulate calcium signalling and mitochondrial function, maintaining Ca^{2+} and ROS balance under stress conditions. (Lu et al., 2025) These integrated actions preserve mitochondrial integrity, support cellular differentiation, and enhance resistance to environmental stressors, including ultraviolet radiation and oxidative damage.

Collectively, the convergence of non-genomic signalling and genomic regulation enables 20-*epi* vitamin D to reduce oxidative stress, maintain cellular integrity, and protect against age-related functional decline, highlighting its role as a key mediator of cellular defense mechanisms.

The anti-proliferative effects of the analogue **UG-635** were evaluated and compared to those of calcitriol in the human breast adenocarcinoma MCF7 cell line and in the mouse pre-osteoblast MC3T3-E1 cell line (Fig. 4). MC3T3-E1 cells exhibited greater sensitivity to the growth-inhibitory effects of calcitriol, with significant suppression of cell proliferation observed at a concentration of 10^{-9} M. In contrast, a 10-fold higher concentration of calcitriol (10^{-8} M) was required to reduce the proliferation of MCF-7 cells. Moreover, a 95% inhibition of cell proliferation was achieved after incubation with 10^{-7} M calcitriol in MC3T3-E1 cells, whereas only a 50% inhibition of proliferation was observed in MCF-7 cells after treatment with 10^{-6} M calcitriol. Interestingly, the anti-proliferative activity of **UG-635** was comparable to that of calcitriol in both cell lines tested.

We next evaluated the antiproliferative activity of **UG-635** using a colony formation assay (Fig. 5). The analogue **UG-635** significantly inhibited clonogenic growth and was more potent than the parent compound calcitriol, reducing both colony number and colony area.

To determine whether the antiproliferative activity of the analogue **UG-635** is mediated through the vitamin D receptor (VDR), we examined its effects on primary mouse embryonic fibroblasts (MEFs) derived from either wild-type ($Vdr^{+/+}$) or $Vdr^{-/-}$ mice. Neither **UG-635** nor its parent compound calcitriol inhibited proliferation of $Vdr^{-/-}$ MEFs, whereas both significantly reduced proliferation of $Vdr^{+/+}$ MEFs (Fig. 6).

The ability of **UG-635** to activate VDR-dependent signalling was further supported by its induction of established VDR target genes (Fig. 7). UG-635 and calcitriol were equipotent in stimulating the transcription of *Cyp24a1*, the major enzyme responsible for calcitriol catabolism, and of receptor activator of nuclear factor kappa-B ligand (Rankl), a key regulator of osteoclastogenesis.

2.3. Crystal structure of VDR- UG-635 complex

The binding mode of **UG-635** to VDR was studied by X-ray crystallography of the complex formed between the ligand, the zebrafish VDR ligand binding domain and a coactivator peptide, and compared with those of calcitriol (PDB: 2HC4) (Ciesielski et al., 2007) or the C20 epimer of **UG-635** (PDB: 8CK5) (Gómez-Bouzó et al., 2023). The data collection and refinement statistics of the structure refined at 2.2 Å resolution, are summarized in **Supplementary Table S1**. The overall structure is highly homologous to the VDR-calcitriol and VDR- 25-nitro derivative of calcitriol structures with a root mean square deviations of 0.2–0.3 Å over 238 residues when comparing the Cα atoms of the complexes. **UG-635** is accommodated in the VDR ligand binding pocket with a shift of 0.5 Å of the D-ring due to the inverted geometry of the C20 methyl group compared to calcitriol (Fig. 8A). In all complexes, the A- to D-ring moieties of the ligands adopt the same conformation and form identical contacts with the protein, notably the C1-OH and C3-OH of **UG-635** form similar H-bonds (Fig. 8B **and Supplementary Table S2**). Whereas the ligands side chains of calcitriol and of the C20 epimer of **UG-635** adopt similar conformation, the side chain of **UG-635** takes a different path in the ligand binding pocket (Fig. 8A). Although the two diastereomer have the same molecular weight and differ only in the position of the C20 methyl group, **UG-635** takes a slightly more compact conformation in the LBP resulting in a 2% decrease in the volume of the ligand binding pocket (**Supplementary Table S3**). **UG-635** is better accommodated in the ligand binding pocket than its C20 *epi*mer that only forms weak interactions with the two anchoring histidines, His333 and His423 (3.3 Å and 3.5 Å). In contrast, the nitro group of **UG-635** forms hydrogen bonds with His333 and His423 (2.9 and 3.1 Å). Compared to calcitriol, differences in interactions with VDR are observed for the 17b-aliphatic chains (Fig. 8C **and Supplementary Table S2**). The C20 methyl group of **UG-635** interacts more strongly with His423 and weakly with Leu337 than calcitriol. In addition, the geminal methyl groups and nitro group form stronger interactions with Leu255, Ala259, Val262 and Ala331 and weaker interactions with Val444 compared to calcitriol.

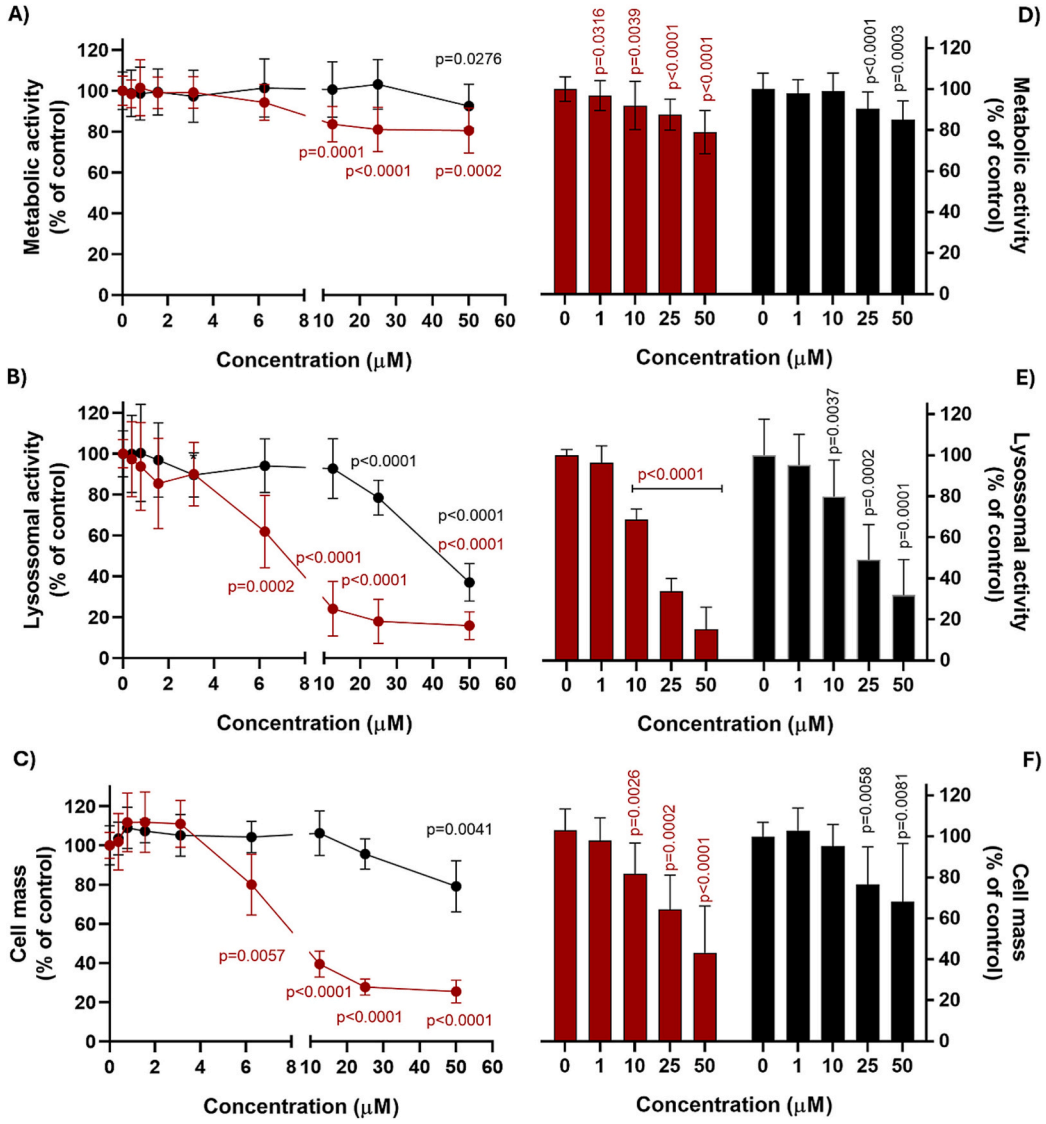

Fig. 2. Cytotoxic profile of the **UG-635** (red data) and **calcitriol** (black data). Differentiated SH-SY5Y cells (left) and HepG2 cells (right) were treated with increasing concentrations (1–50 μM) of compounds and the cytotoxicity was measured based on the metabolic activity (**A**, **D**), lysosomal activity (**B**, **E**) and cell mass (**C**, **F**) 24 h after of treatment. Untreated cells were used as control. Data are expressed as the means of triplicates of at least three independent experiments with the standard deviation (mean ± SD). Statistical comparisons were performed by one-way ANOVA followed by the Dunnett multiple comparison *post hoc* test. In all cases, *p* values lower than 0.05 were considered significant and their exact values are presented in the panels. (For interpretation of the references to colour in this figure legend, the reader is referred to the web version of this article.)

3. Conclusions

In summary, we reported the synthesis and pharmacological evaluation of **UG-635**, a novel 25-nitro-20-*epi*-vitamin D analogue. The compound demonstrated favorable VDR binding, potent antiproliferative effects, and cytoprotective properties against oxidative stress in neuronal cells. These biological activities were comparable or superior to those of calcitriol, with a distinct profile that supports further investigation.

Importantly, the epimeric configuration and C25-nitro substitution may contribute to reduced calcemic risk, as suggested for other 20-*epi* analogues. The structural data also support stronger and more stabilizing interactions within the VDR ligand-binding pocket, potentially enabling a broader therapeutic window.

Overall, **UG-635** represents a promising lead compound for the development of selective vitamin D receptor modulators, with potential applications in oncology and neuroprotection.

4. Experimental section

4.1. Chemistry

NMR spectra were recorded on Bruker ARX-400 or AVANCE DPX400 spectrometers (400 MHz for ^{1}H NMR, 101 MHz for ^{13}C NMR) using TMS as the internal standard. Chemical shifts are reported in δ (ppm) and coupling constants (J) in Hz. Flash column chromatography was performed using silica gel (Merck 60, 230–400 mesh). Analytical TLC was carried out on silica gel plates (Merck 60 F254, 0.25 mm). Mass spectra (ESI) were acquired on a FTMS APEXIII spectrometer. IR spectra were recorded on a Nicolet 6700 FT-IR spectrometer equipped with an ATR accessory and a Smart Orbit diamond crystal. The purity of the final compound was determined by HPLC-DAD equipped with a UV detector (λ = 254 nm) and a silica column (250 × 4.6 mm, 5 μm particle size), using isopropanol/hexane (10:90, *v*/v) as the mobile phase at a flow rate of 4.0 mL/min. Chemical structures and reaction schemes were prepared using ChemDraw Professional (PerkinElmer).

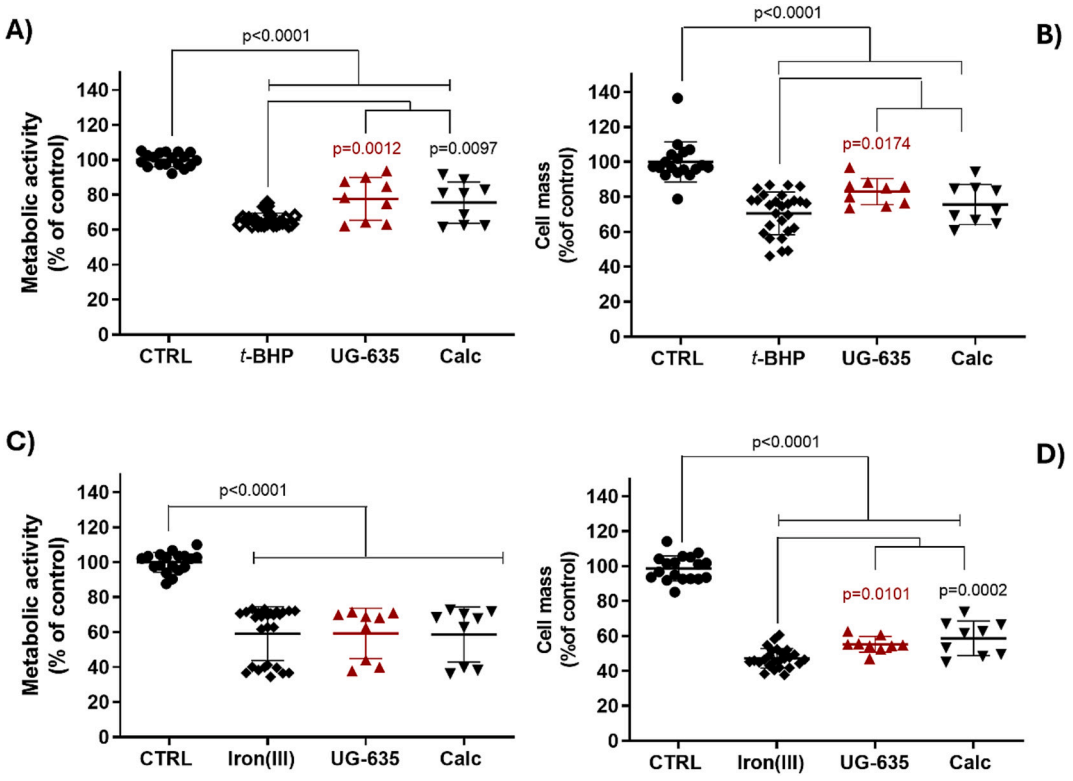

Fig. 3. Evaluation of protection effect of **UG-635** compound and **calcitriol** (labeled as "Calc") at 5 μM in SH-SY5Y cells against using *t*-BHP (**A**, **B**) and FeNTA (**C**, **D**) as oxidative stressors by measuring the metabolic activity (**A**, **C**) and cell mass (**B**, **D**). The data are expressed as the means of triplicates of three independent experiments together with the standard deviation (Mean ± SD). Statistical comparisons were made using two-way ANOVA. In all cases, *p* values lower than 0.05 were considered significant and their exact values are presented in the panels.

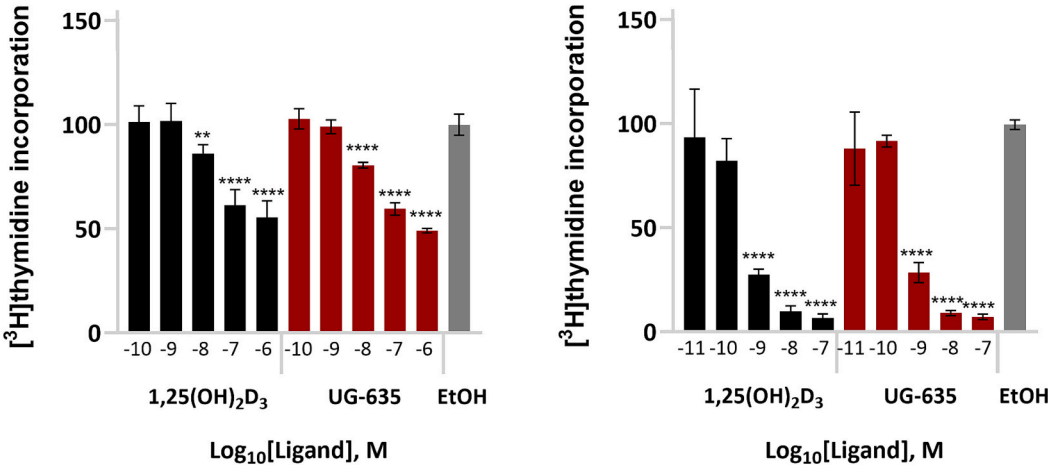

Fig. 4. Anti-proliferative effects of the analogue **UG-635**. Human breast adenocarcinoma MCF-7 cells (left panel) or mouse pre-osteoblast MC3T3-E1 cells (right panel) were treated for 72 h with increasing doses of **calcitriol**, or **UG-635**, after which [^{3}H]thymidine incorporation was measured. Data were analyzed by 1-way-ANOVA. *p* values lower than 0.05 were considered statistically significant, ** $p < 0.01$, **** $p < 0.0001$ *vs.* vehicle (EtOH) treatment.

4.2. Evaluation of biological activity

4.2.1. ABTS radical cation assay

The ABTS$^{\bullet+}$ assay was carried out as described by our group (Fernandes et al., 2018b). The ABTS$^{\bullet+}$ solution was pre-generated by reacting 10 mL of 7 mM ABTS$^{\bullet+}$ aqueous solution and 163 μL of 150 mM (2.45 mM final concentration) potassium persulfate solution. After storage in the dark at room temperature for 16 h, this solution was diluted in EtOH until the absorbance 0.72 ± 0.01 (at 734 nm) was reached. Ethanolic solutions of each compound with different concentrations (5–75 μM) were prepared. Each solution (20 μL) was added to 180 μL of radical solution and absorbance at 734 nm was recorded after 15 min. The radical scavenging activity (%) was calculated as $[(A_C–A_A)/A_C] \times 100$, where A_C and A_A represent the absorbance of the control and antioxidant, respectively. The absorbance of the control (20 μL EtOH and 180 μL of radical solution) was set as 100% radical. Results are presented as means ± standard deviation (SD) of three independent experiments.

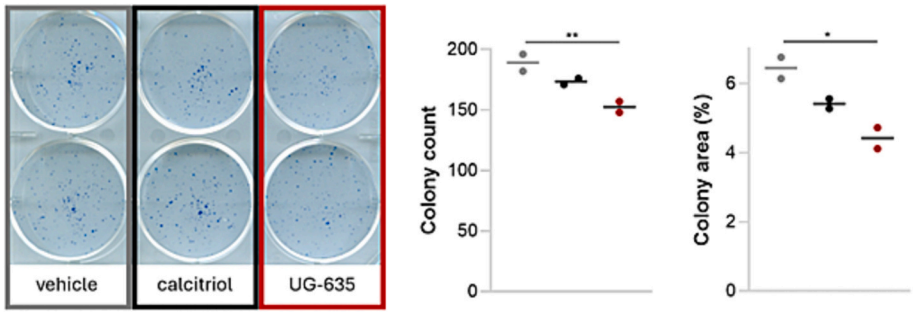

Fig. 5. Effect of the analogue **UG-635** on colony growth. Human breast adenocarcinoma cells were treated with vehicle (EtOH), 10^{-7} M calcitriol or 10^{-7} M **UG-635**. After 48 h of treatment, cells were replated at low density to allow colony formation. After an additional 11 days of culture, colonies were fixed, stained with methylene blue, and quantified. Data were analyzed by 1-way-ANOVA. *p* values lower than 0.05 were considered statistically significant. * $p < 0.05$, ** $p < 0.01$ *vs.* vehicle treatment. (For interpretation of the references to colour in this figure legend, the reader is referred to the web version of this article.)

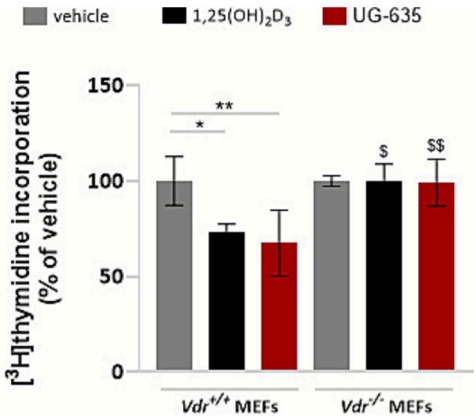

Fig. 6. VDR-signalling mediates the antiproliferative effects of the analogue **UG-635**. Wildtype or $Vdr^{-/-}$ MEFs were treated for 72 h with vehicle (EtOH), 10^{-7} M calcitriol, or 10^{-7} M **UG-635** after which [^{3}H]thymidine incorporation was measured. Data were analyzed by 1-way-ANOVA. *p* lower than 0.05 was considered statistically significant, * $p < 0.05$, ** $p < 0.01$ *vs.* vehicle treatment; \$ $p < 0.05$, \$\$ $p < 0.01$ *vs.* wildtype ($Vdr^{+/+}$) MEFs treated with the same ligand.

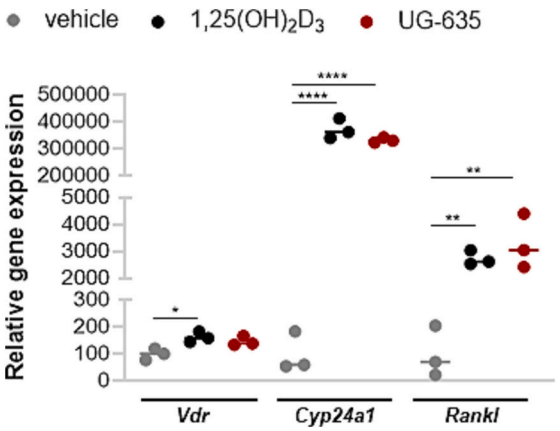

Fig. 7. The analogue **UG-635** induces expression of VDR-target genes. Mouse pre-osteoblast MC3T3-E1 cells were treated with vehicle (EtOH), 3×10^{-8} M calcitriol or 3×10^{-8} M **UG-635**. After 48 h of treatment, RNA was isolated and gene expression was analyzed. Data were analyzed by 1-way-ANOVA. *p* lower than 0.05 was considered statistically significant, * $p < 0.05$, ** $p < 0.01$, **** $p < 0.0001$ *vs.* vehicle treatment.

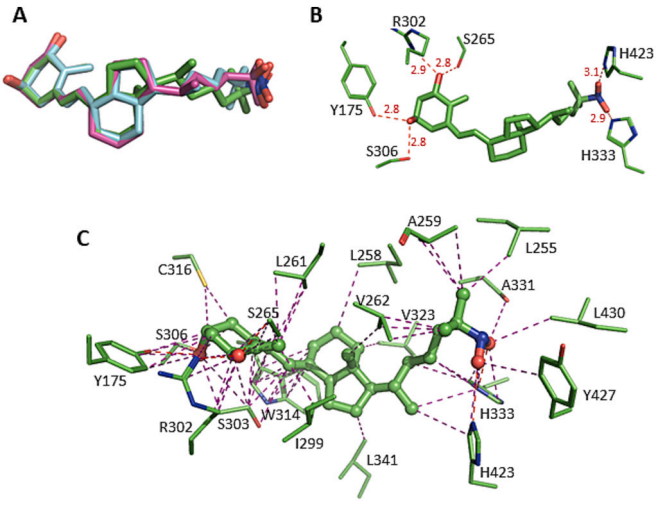

Fig. 8. Crystal structures of zVDR LBD – **UG-635** complex. (**A**) Ligands **UG-635** (PDB: 9RAP) (green), its C20 epimer (PDB: 8CK5) (cyan) superimposed with calcitriol (PDB: 2HC4) (pink). (**B**) Hydrogen bonds formed by **UG-635** are shown by red dotted line. Distances are in Å. (**C**) Interactions of **UG-635** with VDR residues within a 4 Å distance. (For interpretation of the references to colour in this figure legend, the reader is referred to the web version of this article.)

4.2.2. Evaluation of iron chelation activity

The ability of compound **UG-635** to chelate ferrous cations was determined by ferrozine method that is based on the formation of a complex between ferrous cations and ferrozine [3-(2-pyridyl)-5,6-diphenyl-1,2,4-triazine-*p,p'*-disulfonic acid sodium salt (Fernandes et al., 2018b). Compounds that are able to chelate iron prevent the formation of the complex, a process that is translated into an absorbance decrease. The spectrophotometric assay was performed in a multiplate reader (Powerwave XS Microplate Reader) of Bio-Tek instruments. Ethylenediaminetetracetic acid (EDTA) was used as a reference compound. Firstly, 4 μL of compound (20 μM in the well) was joined to 200 μL of a buffer solution (pH = 6.7) of ammonium iron (II) sulfate (20 μM). After 10 min, 4 μL of an aqueous solution of ferrozine (100 μM) was added and the mixture was allowed to react for 10 min. Finally, the amount of complex was determined by spectrophotometry (λ = 532 nm). The iron chelating activity (%) was calculated as $[(A_C–A_A)/A_C] \times 100$, where A_C and A_A represent the absorbance of the control and antioxidant, respectively, after 5 min. The absorbance of the control assay (4 μL of EtOH instead the compound) was set as 0% of iron chelation. Results are presented as means ± SD of three independent experiments.

4.2.3. Cellular studies

Reagents. Reagents used in cell culture such as heat-inactivated fetal bovine serum (FBS), nonessential amino acids (NEAA), 0.25% trypsin/1 mM EDTA, antibiotic (10,000 U/mL penicillin, 10,000 μg/mL streptomycin), phosphate-buffered saline solution (PBS), and Hank's balanced salt solution (HBSS) were purchased from Gibco Laboratories (Lenexa, KS). Neutral red (NR) solution, resazurin, sulforhodamine B (SRB), 0.4% (*w/v*) trypan blue solution, and high-glucose Dulbecco's modified Eagle's medium (DMEM) were acquired from Sigma (St. Louis, MO). Nitrilotriacetic acid disodium salt (Na_2NTA), nitrilotriaceticacetic acid trisodium salt (Na_3NTA), iron (III) chloride and *t*-BHP were acquired from Sigma (Sintra, Portugal). DMSO, MeOH, EtOH, and AcOH were obtained from Merck (Darmstadt, Germany).

4.2.4. Cell culture and conditions

Anti-proliferative assays. The human breast carcinoma (MCF-7) cell line and the mouse MC3T3-E1 (pre) osteoblast were obtained from the American Tissue Culture Company (Rockville, MD). Murine embryonic fibroblasts (MEFs) were isolated from 13-day-old wildtype or Vdr−/− embryos as described by Durkin et al. (Durkin et al., 2013) (PMID: 27376106) *Vdr*−/− mice were purchased from the Jackson Laboratory (JAX Stock # 006133) (Li et al., 1997) (PMID: 9275211). All animal experiments were approved by the ethical committee of the KU Leuven (P188/2016). Cells were seeded in 96-well plates in DMEM medium (MCF-7 and MEFs, 10,000 cells per well) or in alphaMEM medium (MC3T3-E1, 5000 cells/well). Cell culture media were supplemented with 10% fetal bovine serum, 2 mM glutamax, 100 U/mL penicillin, and 100 μg/mL streptomycin (all from Fisher Scientific). The following day, cells were incubated for 72 h with vehicle (ethanol) or increasing concentrations of calcitriol, or **UG-635**. Thereafter, 1 μCi [methyl-^{3}H] thymidine (ICN Biomedicals, Costa Mesa, CA) was added to the cultures and cells were semi-automatically harvested on filterplates after an additional 4 h of incubation (GF/C Filter and Filtermate Universal Harvester, Packard Instrument, Meriden, CT). Counting was performed using a microplate scintillation counter (Topcount, Packard). *Colony formation assay.* MCF-7 cells (2×10^6) were seeded in 75 cm^2 culture flasks and treated the following day with vehicle (ethanol), 10^{-7} M calcitriol or 10^{-7} M **UG-635**. After 48 h of treatment, cells were harvested, counted, and replated in 6-well dishes at a density of 2000 cells per well. Colonies were allowed to form for 11 days, after which they were fixed and stained with methylene blue. Colony number and colony area were quantified from scanned images using ImageJ software. *Gene expression analysis.* MC3T3-E1 cells were seeded in 12-well dishes (40,000 cells/well) and stimulated the following day with vehicle (ethanol), 3×10^{-8} M calcitriol, or 3×10^{-8} M **UG-635**. After 48 h of treatment, RNA was isolated with the InnuPREP RNA isolation kit (Westburg, Leusden, The Netherlands). One μg of RNA was converted into cDNA using oligo(dT) primers and SuperScript II reverse transcriptase (Invitrogen). Gene expression was assessed in triplicate by qRT-PCR using Taqman Fast Universal PCR master mix (Applied Biosystems). Ct values were measured on a QuantStudio 3 (Applied Biosystems) and relative gene expression was calculated with the 2-ΔΔCt method. Expression levels of the genes of interest (*Vdr*, *Cyp24a1*, and *Rankl*) were normalized to the average expression levels of the house keeping gene β-actin.

4.2.5. Cytotoxicity and oxidative stress assays

The cytotoxicity evaluation of the synthetized compounds was performed using human neuroblastoma (SH-SY5Y) and hepatocellular carcinoma (HepG2) cell lines. SH-SY5Y cells (ATCC, Manassas, VA) were routinely cultured in 25-cm^2 flasks (Corning Costar, Corning, NY) using DMEM with 4.5 g/L glucose, supplemented with 10% (*v*/v) heat-inactivated FBS, 1% (v/v) NEAA, and 100 U/mL penicillin and 100 μg/mL streptomycin. Cells were incubated in a humidified atmosphere (5% CO_2–95% air atmosphere) at 37 °C, and the medium was changed every 3 days. The cells were subcultured weekly by trypsinization (0.25% trypsin/1 mM EDTA) and, for all of the experiments, cells were taken between the 19th and 26th passages to avoid phenotypic changes. SH-SY5Y cells were seeded at a density of 25,000 cells/cm^2 in cell culture medium, which was supplemented with 10 μM of retinoic acid (RA) for three days and 80 nm of 12-*O*-tetradecanoylphorbol-13-acetate (TPA) for an additional three days, to promote a dopaminergic differentiation, and incubated at 37 °C in a humidified atmosphere (5% CO_2–95% air atmosphere). (Pinto et al., 2024) SH-SY5Y cells were used 6 days after seeding for all experiments. HepG2 cells (ECACC, U.K.) were routinely cultured in 75 cm^2 flasks using DMEM with 5 mM glucose, supplemented with 6 mM of glutamine, 5 mM 4-(2-hydroxyethyl)-1-piperazineethanesulfonic acid (HEPES), 44 mM sodium bicarbonate, 1 mM sodium pyruvate, 10% FBS, 100 U/mL penicillin and 100 μg/mL streptomycin. HepG2 cells were seeded at a density of 62,500 cells/cm^2 and used the day after seeding. All the experiments were between the 20th and 30th passages.

4.2.6. Cytotoxicity evaluation

The cytotoxicity of the compounds under study (0–50 μM) was evaluated in both HepG2 and differentiated SH-SY5Y cells with the neutral red (NR) uptake, resazurin reduction and SRB binding assays. In the NR uptake assay, 24 h after exposure with the compounds, the cell culture medium was removed and replaced with fresh cell culture medium containing 50 μg/mL of the NR dye, and the cells were incubated at 37 °C in a humidified 5% CO_2–95% air atmosphere for 1 h. Then, the cell culture medium was removed and a mixture of EtOH/H_2O (1:1, *v*/v), containing 5% (*v*/v) AcOH was added to extract the dye accumulated within the lysosomes of living cells. Absorbance was measured at 540 nm in a microplate reader (Synergy HTX Multi-Mode Reader; BioTek, Winooski, VT). In the resazurin reduction assay, 24 h after exposure with the compounds, cell culture medium was removed and replaced with fresh cell culture medium containing 10 μg/mL of resazurin. After 1 h of incubation at 37 °C in a humidified 5% CO_2–95% air atmosphere, the fluorescence was read in a microplate reader using an excitation wavelength of 540 nm and emission of 590 nm. In the SRB binding assay, 24 h after exposure to the compounds the medium was removed, cells were washed with PBS (1×), and fixed overnight at −20 °C with 1% (v/v) AcOH/MeOH. The fixing medium was then removed, and cells incubated with a 0.05% SRB solution for 1 h at 37 °C in a humidified 5% CO_2–95% air atmosphere. Cells were washed with 1% (v/v) aq. AcOH solution (to eliminate unbounded dye), and a 10 mM Tris buffer (pH 10.5) was added to extract the bound SRB. The absorbance at 510 nm was measured in a microplate reader. The results are expressed as resazurin reduction, NR uptake, and SRB binding percentages for resazurin, NR, and SRB, respectively, using untreated cells as control (100% of cell viability).

4.2.7. Protective effects against oxidative stress-induced damage

The antioxidant efficacy of the compounds under study was evaluated in SH-SY5Y cells against well-known oxidative stress inducers such as ferric nitrilotriacetate (FeNTA) and *t*-BHP. Briefly, differentiated SH-SY5Y cells were pretreated with the test compounds (30 min) and then incubated with FeNTA or *t*-BHP. The experimental conditions with the oxidizing agents were firstly optimized and the concentration of each test compound (5 μM) was selected based on their non-cytotoxic effects observed after 24 h, on the NR uptake assay. Nitrilotriacetate (NTA) solution was prepared by mixing nitrilotriacetic acid disodium salt (Na_2NTA) solution (100 mM) and nitrilotriaceticacetic acid trisodium salt (Na_3NTA) solution (100 mM) until pH 7.0 was achieved. The NTA solution was then added to $FeCl_3$ to obtain a final FeNTA solution with 100 mM iron (III) concentration and incubated for 15 min to ensure that the NTA complexed all iron (III). FeNTA was diluted in fresh cell culture medium to obtain a final iron (III) concentration of 50 mM. After a 30 min pretreatment with the compounds, FeNTA (2000 μM) was added, and the cells incubated at 37 °C in a humidified 5% CO_2–95% air atmosphere for 24 h. To evaluate the protective effect of the test compounds against *t*-BHP a fresh stock solution (10 mM) was prepared

(protected from light) in fresh cell culture medium and used immediately. Differentiated SH-SY5Y cells were pretreated with the test compounds for 30 min followed by the addition of *t*-BHP (200 μM), and the cells were then incubated at 37 °C in a humidified 5% CO_2–95% air atmosphere for 24 h. For both assays, following the incubation period, the cytotoxicity induced by the oxidative stressors was evaluated using the resazurin and SRB methods, as described previously. The results are expressed as the mean of non-treated cells as control (100% of cell viability).

Graphs and statistical analyses were performed using GraphPad Prism (GraphPad Software).

4.3. Biochemistry, crystallization, and structure determination

The cDNA encoding His-tagged zVDR LBD (156–453) was cloned into pET28b. The recombinant proteins were produced in Escherichia coli BL21 DE3 grown ON at 18 °C after induction with 1 mM IPTG at an OD600 of ~0.7. Soluble proteins were purified on Ni Hitrap FFcrude column (Cytiva), followed by His tag removal by thrombin cleavage and by size exclusion chromatography on HiLoad Superdex 75 column (Cytiva) equilibrated in 20 mM Tris buffer (pH 7.0), 200 mM NaCl, 1 mM TCEP. The proteins were concentrated to 3–7 mg/mL with an Amicon Ultra 30 kDa MWCO and incubated with a 2-fold excess of ligand and a 3-fold excess of the coactivator NCOA2 NR2 (KHKILHRLLQDSS) peptide. Crystals of VDR/**UG-635** were obtained at 293 K in 3 M sodium acetate and 0.1 M Tris-HCl buffer (pH 8.0). and were mounted in a fiber loop and flash-cooled under a nitrogen flux. Data collection from a single frozen crystal was performed at 100 K on the PX2A at SOLEIL (France). The raw data were processed with XDS (Kabsch, 2010) and scaled with AIMLESS (Evans, 2006) programs. The crystals belong to the space group $P6_522$, with one LBD complex per asymmetric unit. The structures were solved and refined using Buster (Smart et al., 2012), Phenix (Adams et al., 2010), and iterative model building using COOT (Emsley et al., 2010).

Funding

This work was financially supported by the Xunta de Galicia (ED431C-2017/70). U. Gómez-Bouzó acknowledges a predoctoral fellowship from the Xunta de Galicia (ED481A-2021/273). This research was further supported by the French Infrastructure for Integrated Structural Biology (FRISBI) (ANR-10-INBS-05), Instruct-ERIC, and the Agence Nationale de la Recherche under the Investissements d'Avenir program (ANR-10-LABX-0030-INRT and ANR-10-IDEX-0002-02). Portuguese funding was provided by the Foundation for Science and Technology (FCT) and FEDER/COMPETE. S. Barreiro acknowledges support from an FCT doctoral grant (2021.05421.BD). C. Fernandes thanks FCT for financial support through the Scientific Employment Stimulus—Individual Call (10.54499/2021.04016.CEECIND/CP1655/CT0004). L. Verlinden and A. Verstuyf would like to acknowledge the Flanders Research Foundation (FWO; G0D0120N and G081723N).

CRediT authorship contribution statement

Uxía Gómez-Bouzó: Writing – original draft, Visualization, Software, Project administration, Investigation, Data curation, Conceptualization. **Carole Peluso-Iltis:** Methodology, Investigation, Formal analysis. **Sandra Barreiro:** Writing – review & editing, Validation, Methodology, Investigation. **Carlos Fernandes:** Writing – review & editing, Validation, Methodology, Investigation. **Lieve Verlinden:** Writing – review & editing, Visualization, Validation, Methodology, Investigation, Formal analysis. **Annemieke Verstuyf:** Writing – review & editing, Visualization, Validation, Resources. **Fernanda Borges:** Writing – review & editing, Supervision, Resources. **Natacha Rochel:** Writing – review & editing, Visualization, Validation, Methodology, Investigation, Formal analysis. **Generosa Gómez:** Validation, Supervision, Resources, Project administration, Conceptualization. **Yagamare Fall:** Validation, Supervision, Resources, Project administration, Methodology, Funding acquisition.

Declaration of competing interest

The authors declare that they have no known competing financial interests or personal relationships that could have appeared to influence the work reported in this paper.

Acknowledgments

We acknowledge the HPLC, NMR, MS, and IR services of the University of Vigo (CACTI) for technical support. The authors thank Dr. Alastair McEwen (IGBMC) and the staff at the PX2 beamline of the SOLEIL synchrotron for their assistance with X-ray data collection. L. Verlinden and A. Verstuyf thank I. Janssens for excellent technical help.

Appendix A. Supplementary data

Supplementary data to this article can be found online at https://doi.org/10.1016/j.yexmp.2026.105036.

Data availability

Accession Codes. Atomic coordinates for the X-ray structure of zVDR LBD/**UG-635** (PDB: 9RAP) are available from the RCSB Protein Data Bank.

References

Adams, P.D., Afonine, P.V., Bunkoczi, G., Chen, V.B., Davis, I.W., Echols, N., Headd, J.J., Hung, L.W., Kapral, G.J., Grosse-Kunstleve, R.W., et al., 2010. PHENIX: a comprehensive Python-based system for macromolecular structure solution. Acta Crystallogr. D Biol. Crystallogr. 66, 213–221. https://doi.org/10.1107/S0907444909052925.

Binderup, L., Latini, S., Binderup, E., Bretting, C., Calverley, M., Hansen, K., 1991. 20-EPI-vitamin D_3 analogues: a novel class of potent regulators of cell growth and immune responses. Biochem. Pharmacol. 42, 1569–1575. https://doi.org/10.1016/0006-2952(91)90426-6.

Chaiprasongsuk, A., Janjetovic, Z., Kim, T.-K., Li, W., Tuckey, R.C., Slominski, A.T., et al., 2019. Protective effects of novel derivatives of vitamin D_3 and lumisterol against UVB-induced damage in human keratinocytes involve activation of the Nrf2 and p53 defense mechanisms. Redox Biol. 26, 101206. https://doi.org/10.1016/j.redox.2019.101206.

Ciesielski, F., Rochel, N., Moras, D., 2007. Adaptability of the vitamin D nuclear receptor to the synthetic ligand Gemini: remodelling the LBP with one side chain rotation. J. Steroid Biochem. Mol. Biol. 103, 235–242. https://doi.org/10.1016/j.jsbmb.2006.12.003.

Dilworth, F.J., Calverley, M.J., Makin, H.L.J., Jones, G., 1994. Increased biological activity of 20-EPI-1,25-dihydroxyvitamin D_3 is due to reduced catabolism and altered protein binding. Biochem. Pharmacol. 47, 987–993. https://doi.org/10.1016/0006-2952(94)90409-X.

Durkin, M.E., Qian, X., Popescu, N.C., Lowy, D.R., 2013. Isolation of mouse embryo fibroblasts. Bio Protoc 3, e908. https://doi.org/10.21769/BioProtoc.908.

Eelen, G., Verlinden, L., De Clercq, P., Vandevalle, M., Bouillon, R., Verstuyf, A., 2006. Vitamin D analogs and coactivators. Anticancer Res. 26, 2717–2721. https://ar.iiarjournals.org/content/26/4A/2717.short.

Emsley, P., Lohkamp, B., Scott, W.G., Cowtan, K., 2010. Features and development of Coot. Acta Crystallogr. D Biol. Crystallogr. 66, 486–501. https://doi.org/10.1107/S0907444910007493.

Evans, P., 2006. Scaling and assessment of data quality. Acta Crystallogr. D Biol. Crystallogr. 62, 72–82. https://doi.org/10.1107/S0907444905036693.

Fernandes, C., Benfeito, S., Amorim, R., Teixeira, J., Oliveira, P.J., Remião, F., Borges, F., 2018a. Desrisking the cytotoxicity of a mitochondriotropic antioxidant based on caffeic acid by a PEGylated strategy. Bioconjug. Chem. 29, 2723–2733. https://doi.org/10.1021/acs.bioconjchem.8b00383.

Fernandes, C., Pinto, M., Martins, C., Gomes, M.J., Sarmento, B., Oliveira, P.J., Remião, F., Borges, F., 2018b. Development of a PEGylated-based platform for efficient delivery of dietary antioxidants across the blood–brain barrier. Bioconjug. Chem. 29, 1677–1689. https://doi.org/10.1021/acs.bioconjchem.8b00151.

Ferronato, M.J., Obiol, D.J., Alonso, E.N., Guevara, J.A., Grioli, S.M., Mascaró, M., Rivadulla, M.L., Martínez, A., Gómez, G., Fall, Y., et al., 2019. Synthesis of a novel analog of calcitriol and its biological evaluation as antitumor agent. J. Steroid Biochem. Mol. Biol. 185, 118–136. https://doi.org/10.1016/j.jsbmb.2018.08.006.

Fujishima, T., Liu, Z., Miura, D., Chokki, M., Ishizuka, S., Konno, K., Takayama, H., 1998. Bioorg. Med. Chem. Lett. 8, 2145–2148. https://doi.org/10.1016/S0960-894X(98)00363-1.

Gómez-Bouzó, U., Belorusova, A.Y., Rivadulla, M.L., Santalla, H., Verlinden, L., Verstuyf, A., Ferronato, M.J., Curino, A.C., Facchinetti, M.M., Fall, Y., et al., 2023. Structural analysis and biological activities of C25-amino and C25-nitro vitamin D analogs. Bioorg. Chem. 136, 106528–106533. https://doi.org/10.1016/j.bioorg.2023.106528.

Kabsch, W., 2010. Software XDS for image rotation, recognition and crystal symmetry assignment. Acta Crystallogr. D Biol. Crystallogr. 66, 125–132. https://doi.org/10.1107/S0907444909047337.

Li, Y.C., Pirro, A.E., Amling, M., Delling, G., Baron, R., Bronson, R., Demay, M.B., 1997. Targeted ablation of the vitamin D receptor: an animal model of vitamin D-dependent rickets type II with alopecia. Proc. Natl. Acad. Sci. U. S. A. 94, 9831–9835. https://doi.org/10.1073/pnas.94.18.9831.

Lu, M., Zhan, Z., Li, D., Chen, H., Li, A., Hu, J., Huang, Z., Yi, B., 2025. Protective role of vitamin D receptor against mitochondrial calcium overload from PM(2.5)-induced injury in renal tubular cells. Redox Biol. 80, 103518–103535. https://doi.org/10.1016/j.redox.2025.103518.

Nowak, J.I., Olszewska, A.M., Wierzbicka, J.M., Gebert, M., Bartoszewski, R., Żmijewski, M.A., 2023. VDR and PDIA3 are essential for activation of calcium signaling and membrane response to 1,25(OH)(2)D(3) in squamous cell carcinoma cells. Cells 13, 11–24. https://doi.org/10.3390/cells13010011.

Patel, R., Nandini, Kharkwal, H., Saha, M., Sankaranarayanan, M., Sharma, S., Chander, S., 2025. Recent advancements towards the use of vitamin D isoforms and the development of their synthetic analogues as new therapeutics. Biomedicines 13, 1002–1035. https://doi.org/10.3390/biomedicines13041002.

Pinto, M., Silva, T.B., Sardão, V.A., Simões, R., Albuquerque, B., Oliveira, P.J., Valente, M.J., Remião, F., Soares-da-Silva, P., Fernandes, C., Borges, F., 2024. Cellular and mitochondrial toxicity of tolcapone, entacapone, and new nitrocatechol derivatives. ACS Pharmacol. Transl. Sci. 7, 1637–1649. https://doi.org/10.1021/acsptsci.4c00124.

Posner, G.H., Kahraman, M., 2003. Organic chemistry of vitamin D analogues (deltanoids). Eur. J. Org. Chem. 2003, 3889–3895. https://doi.org/10.1002/ejoc.200300264.

Rivadulla, M.L., Pérez-García, X., Pérez, M., Gómez, G., Fall, Y., 2013. Pd-allylic substitution mediated synthesis of 25-amino vitamin D_3 derivatives. Tetrahedron Lett. 54, 3164–3166. https://doi.org/10.1016/j.tetlet.2013.04.019.

Rochel, N., Moras, D., 2011. Structural basis for ligand activity in VDR. In: Feldman, D., Pike, J.W., Adams, J.S. (Eds.), Vitamin D, third ed. Academic Press, Amsterdam.

Rochel, N., Wurtz, J.M., Mitschler, A., Klaholz, B., Moras, D., 2000. The crystal structure of the nuclear receptor for vitamin D bound to its natural ligand. Mol. Cell 5, 173–179. https://doi.org/10.1016/S1097-2765(00)80413-X.

Slominski, A.T., Chaiprasongsuk, A., Janjetovic, Z., Kim, T.-K., Stefan, J., Slominski, R. M., Hanumanthu, V.S., Raman, C., Qayyum, S., Song, Y., et al., 2020. Photoprotective properties of vitamin D and Lumisterol Hydroxyderivatives. Cell Biochem. Biophys. 78, 165–180. https://doi.org/10.1007/s12013-020-00913-6.

Slominski, A.T., Brożyna, A.A., Kim, T.-K., Elsayed, M.M., Janjetovic, Z., Qayyum, S., Slominski, R.M., Oak, A.S.W., Li, C., Podgorska, E., et al., 2022. CYP11A1-derived vitamin D hydroxyderivatives as candidates for therapy of basal and squamous cell carcinomas. Int. J. Oncol. 61, 96. https://doi.org/10.3892/ijo.2022.5386.

Slominski, A.T., Kim, T.-K., Janjetovic, Z., Slominski, R.M., Li, W., Jetten, A.M., Indra, A. K., Mason, R.S., Tuckey, R.C., 2024a. Biological effects of CYP11A1-derived vitamin D and Lumisterol metabolites in the skin. J. Invest. Dermatol. 144, 2145–2161. https://doi.org/10.1016/j.jid.2024.04.022.

Slominski, R.M., Kim, T.-K., Janjetovic, Z., Brożyna, A.A., Podgorska, E., Dixon, K.M., Mason, R.S., Tuckey, R.C., Sharma, R., Crossman, D.K., et al., 2024b. Malignant melanoma: an overview, new perspectives, and vitamin D signaling. Cancers 16, 2262. https://doi.org/10.3390/cancers16122262.

Smart, O.S., Womack, T.O., Flensburg, C., Keller, P., Paciorek, W., Sharff, A., Vonrhein, C., Bricogne, G., 2012. Exploiting structure similarity in refinement: automated NCS and target-structure restraints in BUSTER. Acta Crystallogr. D Biol. Crystallogr. 68, 368–380. https://doi.org/10.1107/S0907444911056058.

Voltan, G., Cannito, M., Ferrarese, M., Ceccato, F., Camozzi, V., 2023. Vitamin D: an overview of gene regulation, ranging from metabolism to genomic effects. Genes 14, 1691–1706. https://doi.org/10.3390/genes14091691.